



City Research Online

City, University of London Institutional Repository

Citation: Nouri, J. M. & Hockey, R. (2008). Flow characteristics of Newtonian and non-Newtonian fluids in a vessel stirred by a 60° pitched blade impeller. *The International Journal of Multiphysics*, 2(1), pp. 83-105. doi: 10.1260/175095408784300261

This is the published version of the paper.

This version of the publication may differ from the final published version.

Permanent repository link: <https://openaccess.city.ac.uk/id/eprint/13226/>

Link to published version: <https://doi.org/10.1260/175095408784300261>

Copyright: City Research Online aims to make research outputs of City, University of London available to a wider audience. Copyright and Moral Rights remain with the author(s) and/or copyright holders. URLs from City Research Online may be freely distributed and linked to.

Reuse: Copies of full items can be used for personal research or study, educational, or not-for-profit purposes without prior permission or charge. Provided that the authors, title and full bibliographic details are credited, a hyperlink and/or URL is given for the original metadata page and the content is not changed in any way.

City Research Online:

<http://openaccess.city.ac.uk/>

publications@city.ac.uk

Flow characteristics of Newtonian and non-Newtonian fluids in a vessel stirred by a 60° pitched blade impeller

Jamshid M Nouri* and **Randal Hockey**

City University London, School of Engineering and Mathematical Sciences,
Northampton Square, London EC1V 0HB, UK

ABSTRACT

Mean and rms velocity characteristics of two Newtonian flows at Reynolds numbers of 12,800 (glycerin solution) and 48,000 (water) and of a non-Newtonian flow (0.2% CMC solution, at a power number similar to the Newtonian glycerin flow) in a mixing vessel stirred by a 60° pitched blade impeller have been measured by laser Doppler velocimetry (LDV). The velocity measurements, resolved over 360° and 1.08° of impeller rotation, showed that the mean flow of the two power number matched glycerin and CMC flows were similar to within 3% of the impeller tip velocity and the turbulence intensities generally lower in the CMC flow by up to 5% of the tip velocity. The calculated mean flow quantities showed similar discharge coefficient and pumping efficiency in all three flows and similar strain rate between the two power number matched glycerin and CMC flows; the strain rate of the higher Reynolds number Newtonian flow was found to be slightly higher. The energy balance around the impeller indicated that the CMC flow dissipated up to 9% more of the total input power and converted 7% less into the turbulence compared to the glycerin flow with the same power input which could lead to less effective mixing processes where the micro-mixing is important.

Keywords: Newtonian and non-Newtonian flows; Turbulent; Mixing vessel; 60° pitched-blade impeller; LDV system

1. INTRODUCTION

Mixing processes in stirred vessels have many applications in chemical engineering and often involve liquid-liquid blending and solid suspension in liquid. The liquids used are often non-Newtonian in nature like shear thinning behavior, time dependency, visco-elasticity or have a finite yield stress. In general, mixing processes are very complex as the flow is three-dimensional, often turbulent, multi-phase and the fluids are non-Newtonian. Thus, a better understanding of the mixing process involves not only knowledge of the material properties and reaction rates, but also of the details of the flow. The present experimental work is therefore aimed at quantifying and comparing the flow and power characteristics of a Newtonian fluid

*Corresponding author: j.m.nouri@city.ac.uk

(glycerin solution) and of an aqueous polymer solution (0.2% solution of Carboxymethyl Cellulose Sodium salt, brand name CMC, grade 7H4C from Hercules) generated by a 60° pitched blade impeller. Laser Doppler velocimeter has been used to measure the mean and rms of the three velocity components resolved over 360° and 1.08° of the impeller rotation in the bulk region of the vessel and around the impeller, respectively; the induced torque was measured by an air bearing.

Previous experimental studies on Newtonian flow characteristics in mixing vessels generated by pitched blade impellers have been discussed in details by [1]. In brief, the experimental of [2] reported velocity measurements for a 45° pitched blade impeller using LDV and showed that the maximum axial velocity is half of the tip velocity and that the tangential velocity was proportional to the radius. The results of [3] were more detailed and revealed that the velocities scaled with rotational speed and that the hydraulic efficiency increases with the blade pitch. The studies of [4-5] also used 45° pitched-blade impellers and showed the bulk flow patterns are different for low and high off-bottom clearances. Detailed time-resolved LDV measurements by [1] for a 60° pitched blade impeller revealed an axial jet which originated beneath the impeller and formed a large ring vortex covering up to two thirds of the vessel height, a small vortex was shed from the tip of each blade which decayed rapidly, a swirl velocity beneath the impeller proportional to radius and that the turbulence in the discharge region was in general anisotropy. They also showed that the effect of the blade passage was present mainly in the impeller discharge jet up to a distance twice the blade width away from the blade tip. The pumping efficiency of the pitched blade impeller was found to be 2.5 times higher than a Rushton type impeller of the same size, while it dissipated less power within the impeller. Investigations of [6] and [7] used 2-D and 3-D PIV techniques in mixing vessels stirred with 45° pitched blade and Rushton impellers, respectively, to estimate the turbulent dissipation rate and made comparison with previous estimated values made from single-point velocity measurement techniques. In particular, the former investigation showed that for a coarse spatial resolution of 5 mm the estimated rate of dissipation agrees well with that of the dimensional analysis employed by [5]. The latter study showed the feasibility of direct measurement of the dissipation distribution using both 2-D and 3-D PIV methods by measuring the mean velocities and Reynolds stresses simultaneously from which the dissipation rate was determined. They showed that values of the normalized ensemble-averaged dissipation rate in the impeller stream were in the range 5–10%, and that the measured values compared well with those of earlier works employing non-direct methods showing that some of those methods yielded comparable values.

Experimental investigations of non-Newtonian fluids were mainly concerned on flow visualisation and power characteristics, for example, [8-9] who visualized the flow patterns of plastic and pseudoplastic fluids at low Reynolds number, up to 300, and showed that a downwards flow generated by a 45° pitched blade impeller produced more circulation than that of an upward flow, but the aeration with the former flow took place at significantly lower impeller speed. Power measurements by [10] showed good agreement between the power number of the Newtonian and shear-thinning polymer (CMC) solutions in the turbulent flow with similar values and that the CMC solution had the effect of delaying the discharge flow transition (from radial to axial) to a higher Reynolds number with higher concentration causing more of a delay.

Flow visualisation technique was also used by [11-12] to investigate flow characteristics of pseudo-plastic and visco-elastic fluids in mixing vessels in the laminar and up to transitional flows. The former investigation [11] confirmed the finding of the earlier work by [13], who proposed a linear relation between the tank average shear, $\dot{\gamma}$, rate and the impeller



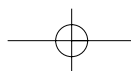
speed, N , with Rushton impeller in the laminar flow for both Newtonian and non-Newtonian fluids as $\dot{\gamma} = k_s N$ where k_s is the shearing constant with a value of 12 for the pitched-blade impeller. The mean flow visualisation of [12] revealed the radial to axial discharge flow transition, as mentioned above, with non-Newtonian fluids and concluded that this was an elastic effect. The flow visualisation of [14] also confirmed this flow transition, but they showed that this happened with both Newtonian and non-Newtonian fluids and concluded that this was a Reynolds number or viscosity effect. This was confirmed by the velocity measurements of [15] who measured the flow velocities before and after the transitions for both Newtonian and 0.2% CMC shear-thinning fluids. This flow transition changed the overall flow pattern in the mixing vessel from a double vortical structure to a single large vortex with a sudden reduction in power consumption by about 12% [10]; similar sudden drop in power was reported by the measurements of [16] who used a different power measuring technique to that used in the present study.

Non-Newtonian fluid effects, such as shear-thinning and elasticity, on power consumption in mixing vessels stirred with other types of impellers than pitched-blade were investigated by [17] and [18] who used a helical ribbon and double planetary mixers, respectively. The former study showed that in the laminar flow there is no effect of elasticity on the power consumption at low Reynolds number, Re , while at the higher value of Re the fluid elasticity caused an increase in power consumption. The latter study, with double planetary mixers, [18] found the value of constant k_s depended on the level of fluid shear thinning in such a way that as the fluids became more shear-thinning then k_s has to be decreased. The recent work of [19] used hyperboloid impellers and showed that the shearing constant with this type of impeller was around 27.2 and that the power consumption was reduced with elastic fluids especially with CMC solutions by up to 13% compared to that of Newtonian fluids; it was speculated that this reduction in power was similar to that of drag reduction with non-Newtonian fluids in the pipe. They have also measured the flow field velocity with LDV and revealed that CMC solutions caused a reduction in flow circulation by up to 25% and that the rms fluctuating velocities were, in general, lower than that of Newtonian fluid; more elastic fluids caused high reduction in circulation and rms level.

In the present study the mean and rms velocities have been obtained in the glycerin and 0.2% CMC flows with the same power input for proper comparison and scaling purposes. The results are made in great detail so that they can be used for the appraisal of the CFD models. The flow configuration and experimental techniques are described in the following section, the results are presented and discussed in section 3, and the paper ends with a summary of findings.

2. FLOW CONFIGURATION AND INSTRUMENTATION

The mixing vessel, shown in figure 1, was the same as that used by [1] and made from a clear Perspex cylinder of inside diameter $T = 294\text{mm}$ equal to the liquid height, H , with four baffles of width and thickness of $T/10$ and $T/100$, respectively; a lid was used on the vessel to avoid air entrainment from the free surface. The stirrer was a 60° pitched blade impeller with six blades, a diameter of $D = T/3$ and a clearance from the base of the vessel of $C = T/3$; the details of the impeller are also shown in figure 1 with blade thickness of 3 mm. The vessel was placed inside a rectangular box, also from Perspex, and the intervening space filled with the same fluid as inside the vessel so as to reduce problems associated with refraction by the curved surface. The vessel was mounted on a traversing bench that allowed translation in three directions with an accuracy of ± 0.025 mm and rotation around z axis with a precision of $\pm 0.25^\circ$.



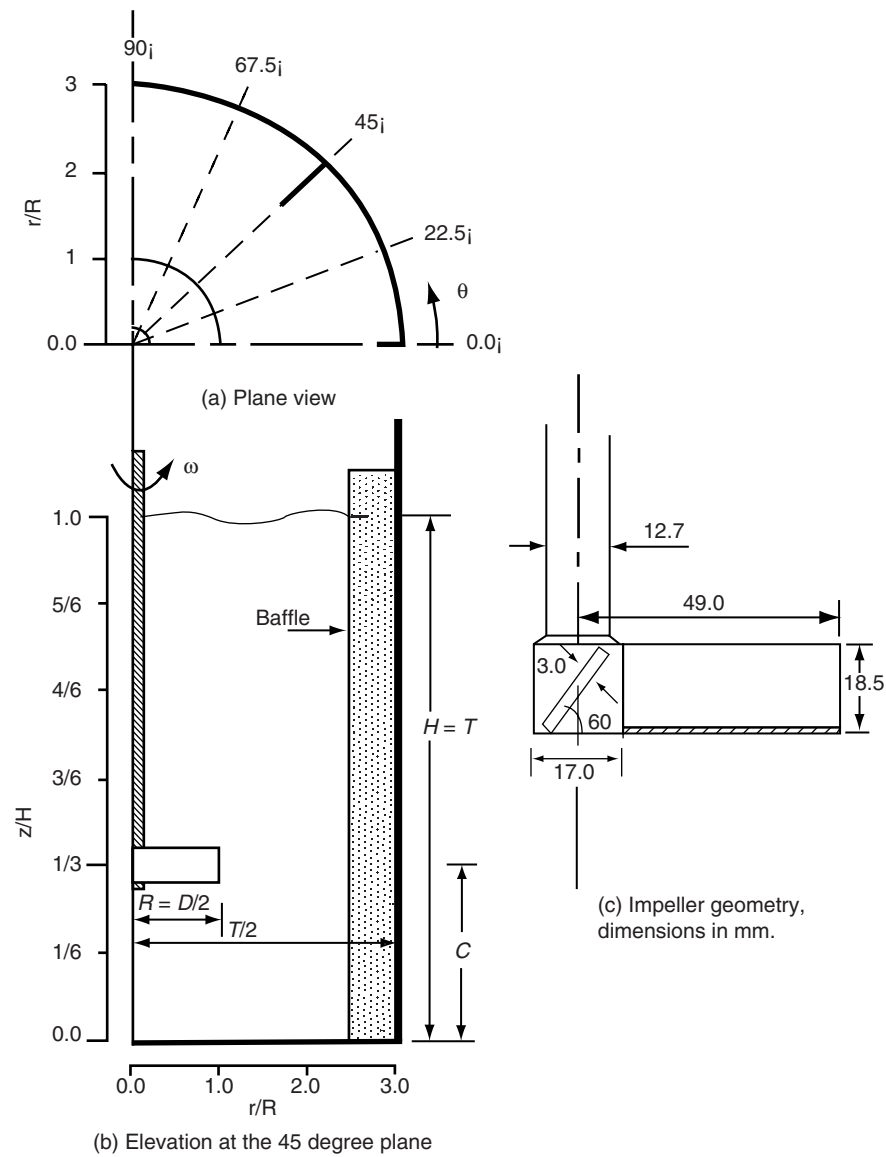


Figure 1 Flow configuration and co-ordinate system for $D = C = T/3$ configuration.

The impeller was driven by a 1.5 kW d.c. motor (GEC MD 112160) and the maximum variation in impeller speed did not exceed ± 0.5 rpm. An optical shaft encoder with a train of 2000 pulses per revolution was used to measure the impeller speed and also to record the position of the impeller blade with a marker pulse to an angular resolution of 0.18° . A mixture of water and glycerin with a density of 1142 kg/m^3 , a kinematic viscosity of 10.1 cS and a dynamic viscosity of 0.0115 Pa.s , was used as the Newtonian fluid for velocity measurements; the same Newtonian fluids as those used by [10] were used for torque measurements. The non-Newtonian fluid was an aqueous solution of Sodium Carboxymethyl Cellulose (CMC, 7H4C from Hercules) CMC, 0.2% solution by weight, which is a weakly elastic shear-thinning polymer.



An important parameter which characterises the performance of impellers is the non-dimensional power number, N_p , that measures the power requirements and is given by

$$N_p = \frac{P}{\rho N^3 D^5} \quad (1)$$

where N is the impeller rotational speed in rev/s, ρ is the fluid density, D is impeller diameter and P is the power input which was calculated from the induced torque (T_r) measurements as $P = \omega T_r$ where ω is the shaft rotational speed in rad/s. The Reynolds number for the Newtonian fluids in stirred vessel is defined as $Re = \frac{ND^2}{\nu}$ where ν is the kinematic viscosity of the fluid. With the 0.2% CMC solution, an effective viscosity was obtained according to the procedure given by Nouri and Hockey (1998) from a power law model in the form of

$$\mu = m\dot{\gamma}^{n-1} = m(k_s N)^{n-1} \quad (2)$$

where k_s is the shearing constant taken as 12, and m and n are the fluid consistency index and the power index which are equal to 0.044 in Pa.s⁻ⁿ and 0.75 for 0.2% CMC solution from the rheological data of [20]. For example at an impeller speed of 800 rpm, the effective dynamic viscosity is 0.0123 Pa.s; i.e. 7% larger than the Newtonian glycerin mixture. It should be mentioned that another viscosity model which is more appropriate for CMC solutions is the simplified Carreau model [17] which was also used by [19] and may result in a better estimate of viscosity than that of the power law model. However, it was shown by [20] that the agreement between the measured and estimated (using the power law) values for the range of shear rate that used in this experiment was very good. In any case, a small deviation in estimation of viscosity will not alter the conclusions that are derived in the present study.

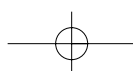
The same measuring techniques as those of [1] are used and the description is not repeated here. In brief, the induced torque was obtained from an air bearing with an overall maximum uncertainty of less than 5%. The laser Doppler velocimeter was operated in the dual-beam forward scatter mode with a 40 mW helium-neon laser. Two equal intensity beams formed a measuring volume of 968 μm in length and 74 μm in diameter, with a fringe spacing of 3.1 μm and a frequency shift of 2.5MHz to remove the directional ambiguity. The signal from photomultiplier was processed by a frequency counter interfaced to a microprocessor and led to ensemble-average values of the mean and rms velocities. Two types of average values were obtained: first, the ensemble-averaged over 360° by collecting data over many impeller rotations in the bulk of the flow and around the impeller. The second type was ensemble-averaged values obtained over 1.08° of impeller rotation, so-called “gated” measurements, around the impeller. The overall maximum uncertainties in mean and rms velocities were 1% and 4% of the impeller tip velocity (V_p), respectively, for the 360° averaging, rising to 2.2 and 12% for the 1.08° averaging.

3. RESULTS AND DISCUSSION

The results of power measurements is presented first and then followed by the flow field velocity measurements made with LDV.

3.1. POWER MEASUREMENTS

The power number results with the Newtonian and 0.2% CMC solutions are presented first to provide the power characteristics of the impeller as a function of Reynolds number as



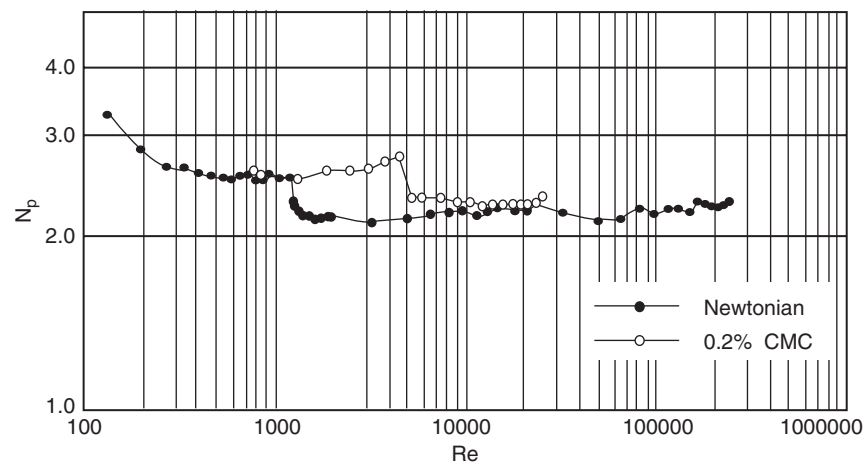


Figure 2 Variation of power number of Newtonian fluid and 0.2% CMC solution as a function of Reynolds number.

shown in figure 2. With the Newtonian fluid, there is a sharp drop of about 12% in power number at a Reynolds number of 1,200 which is associated with a change of discharge flow from radial to axial, and that after this transition the power number remain almost constant with an average value of 2.22 ± 0.04 . Similar flow transition can be seen with the CMC solution but delayed to a higher Reynolds number of 4500 where the power number drops by the same amount as the Newtonian value. The agreement between the power numbers of the Newtonian fluid and 0.2% CMC solution after the transition points in turbulent flow region (i.e. $Re > 10,000$) is good to within 5%.

It is clearly evident, figure 2, that the flow transition with the CMC solution is delayed to a higher Reynolds number, four times that of Newtonian fluid. It was shown, by our earlier work [10], that this delay in transition is a non-Newtonian effect and independent of the method of calculating the apparent Reynolds number. It was also speculated that the increase in elongation viscosity of molecules can be responsible for this delay in a similar manner to that of the drag reduction in duct flows as explained by [21-22].

3.2. VELOCITY MEASUREMENTS

The velocity of the CMC and glycerin flows have been measured and compared on the basis that they generate similar values of the power number, which is the ratio of the flow producing pressure forces to the inertial forces, operate in the same flow regime, i.e. turbulent, and have the same impeller speed to insure similar relative mean velocity between the blades and liquids. Thus, from the results of power number a value of 2.3 in turbulent region was chosen for the CMC solution at a rotational speed of 800 rpm ($Re = 10300$), well past the end of the radial to axial flow transition point at 450 rpm ($Re = 5040$); for the Newtonian fluid (glycerin) this corresponds to a Reynolds number of 12,800. Some water flow results [1] at a Reynolds number of 48,000 ($N = 300$ rpm) are also presented for comparison and scaling purposes. The bulk flow velocity measurements, averaged over 360° and over many impeller rotation, are presented first followed by those obtained around the impeller with respect to impeller rotation, averaged over 1.08° .



3.2.1. Bulk flow measurements

All measurements were made in the $\theta = 0^\circ$ plane with respect to baffle, since there were little circumferential flow variation except around the baffle as was shown by [1]. Behind the baffle in the recirculation zone, tangential velocity at different angular planes was also measured. All velocities are normalised with the impeller tip velocity, V_t , and the radial and axial distances are normalised with the impeller radius, R , and vessel height, H , respectively; the tip velocities for the 0.2% CMC, water and glycerin flows are 4.1, 1.54 and 4.1m/s, respectively.

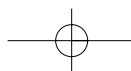
The overall mean flow is presented in figures 3(a) to (d) where the vector additions of the mean axial and radial velocities $\left(\sqrt{\bar{U}^2 + \bar{V}^2}\right)$ and contours of the mean tangential velocity with the glycerin and 0.2% CMC solutions are shown. The results show very similar flow patterns for both fluids with the same impeller jet stream trajectory, the same size of recirculation region below the impeller along the tank base, and the same size of the main recirculation region with its centre at $r = 2.16R$ and $z = 0.25H$. There are, however, small differences that can be seen much better in figure 4 where the profiles of all velocity components with glycerin and 0.2% CMC solutions are presented together with the results for water flow at a Reynolds number of 48,000. The largest differences between the glycerin and CMC solutions occur in the impeller jet where the glycerin flow is slightly stronger so that the axial velocity with the glycerin solution is greater by $0.045V_t$, and the radial and tangential velocities are greater by $0.03V_t$ than with the CMC solutions. This may suggest that the flow with CMC is not yet as developed as the Newtonian flow. Elsewhere in the vessel, the differences in velocity between the glycerol and CMC solutions are small and less than $0.02V_t$.

Comparison between the two Newtonian flows shows the impeller jet at the lower Reynolds number of 12,800 is more inclined outwards by 3° than at 48,000, causing the recirculation region below the impeller along the vessel base to extend out to a radial location of $r = 0.72R$ at $z = 0.068H$, compared to $r = 0.51R$ at 48,000. This is expected as the flow with water is more fully developed with its Reynolds number 3.8 times higher than the glycerin flow. The velocities in this region were generally stronger for the higher Reynolds number with the maximum difference in velocities between the axial components of $0.086V_t$. These differences became smaller away from the impeller so that the maximum differences reduced to about 0.06 and $0.02V_t$ in the wall jet and above the impeller, respectively.

The contours of the tangential velocity below the impeller, figures 3(c) and (d), also show similar swirling velocities with the two power number matched flows and that the swirl velocities of all three flows beneath the impeller, figure 4(c), are proportional to radius. The tangential velocity in the recirculation region behind the baffle at $z = 0.068H$, figure 4(d), shows again that all flows are very similar with the maximum difference occurring in the region of reversed flow and between the two Newtonian fluids; it was larger with the higher Reynolds number by $0.03V_t$.

Overall, the differences between the two Newtonian flows are generally small, as would be expected when operating in the turbulent regime with Reynolds number above 10^4 . The differences between the mean flow of the glycerin and 0.2% CMC solutions are also small, even smaller than those between the Newtonian flows. This similarity in the mean flow is again expected as the impeller speed and power input with both Newtonian and non-Newtonian liquids are the same and also because they have similar apparent viscosities.

The rms of the three velocity components with Newtonian fluids and 0.2% CMC solution is presented in figure 5 and shows little differences between the two Newtonian flows except in the impeller jet region where all three rms velocity components are greater with the higher



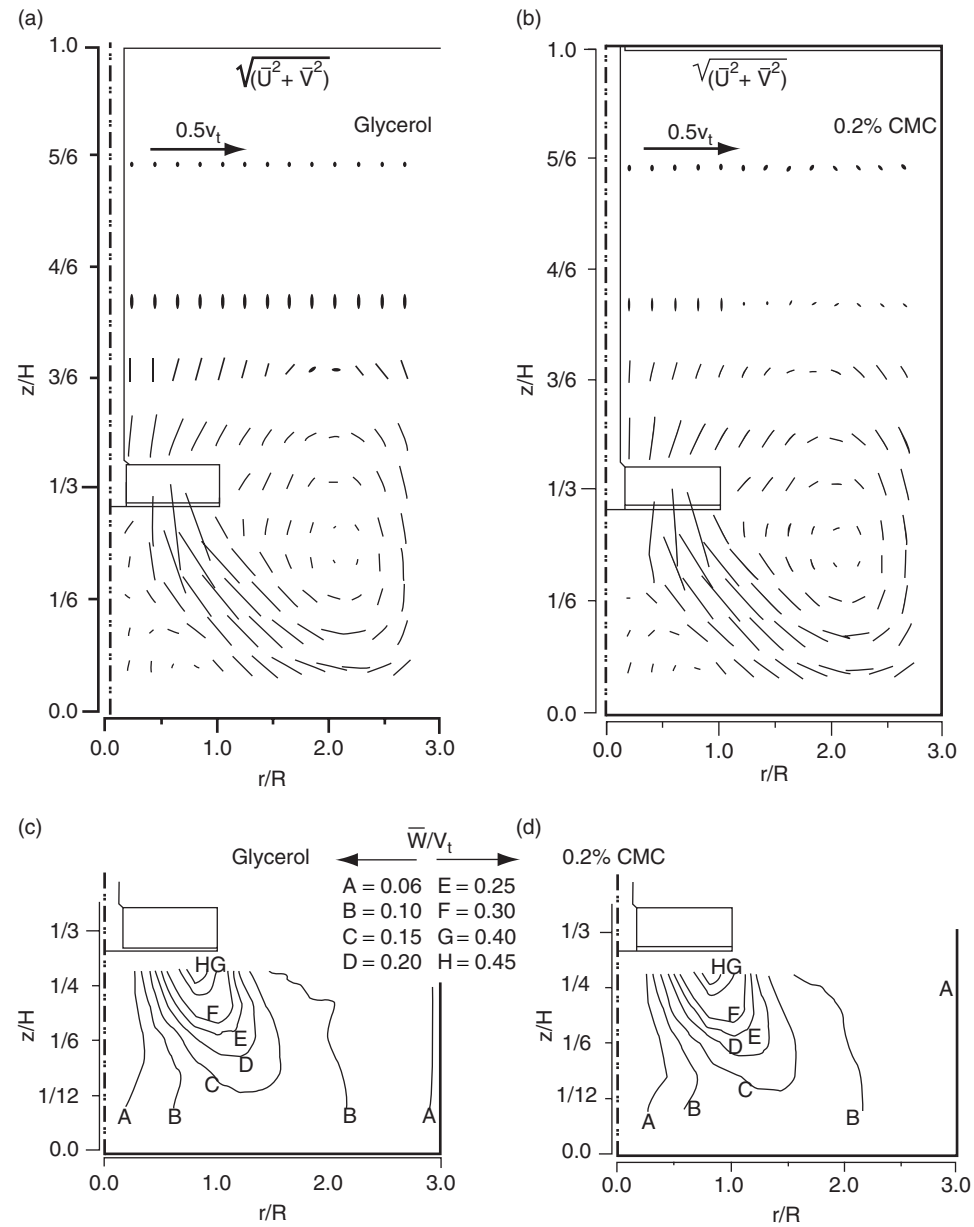


Figure 3 Mean flow velocities of glycerol and 0.2% CMC solution for a power number 2.3, in $\theta = 0^\circ$ plane: (a) & (b) axial and radial velocity vector; (c) & (d) tangential velocity contours.

Reynolds number by around $0.025V_t$. Unlike the mean flow, the differences in rms velocities between the glycerin and 0.2% CMC solutions are larger in which the turbulence intensities with the CMC solution are suppressed. Again, the greatest differences are in the impeller jet, a region of high shearing, where the axial, radial and tangential rms velocities with glycerin

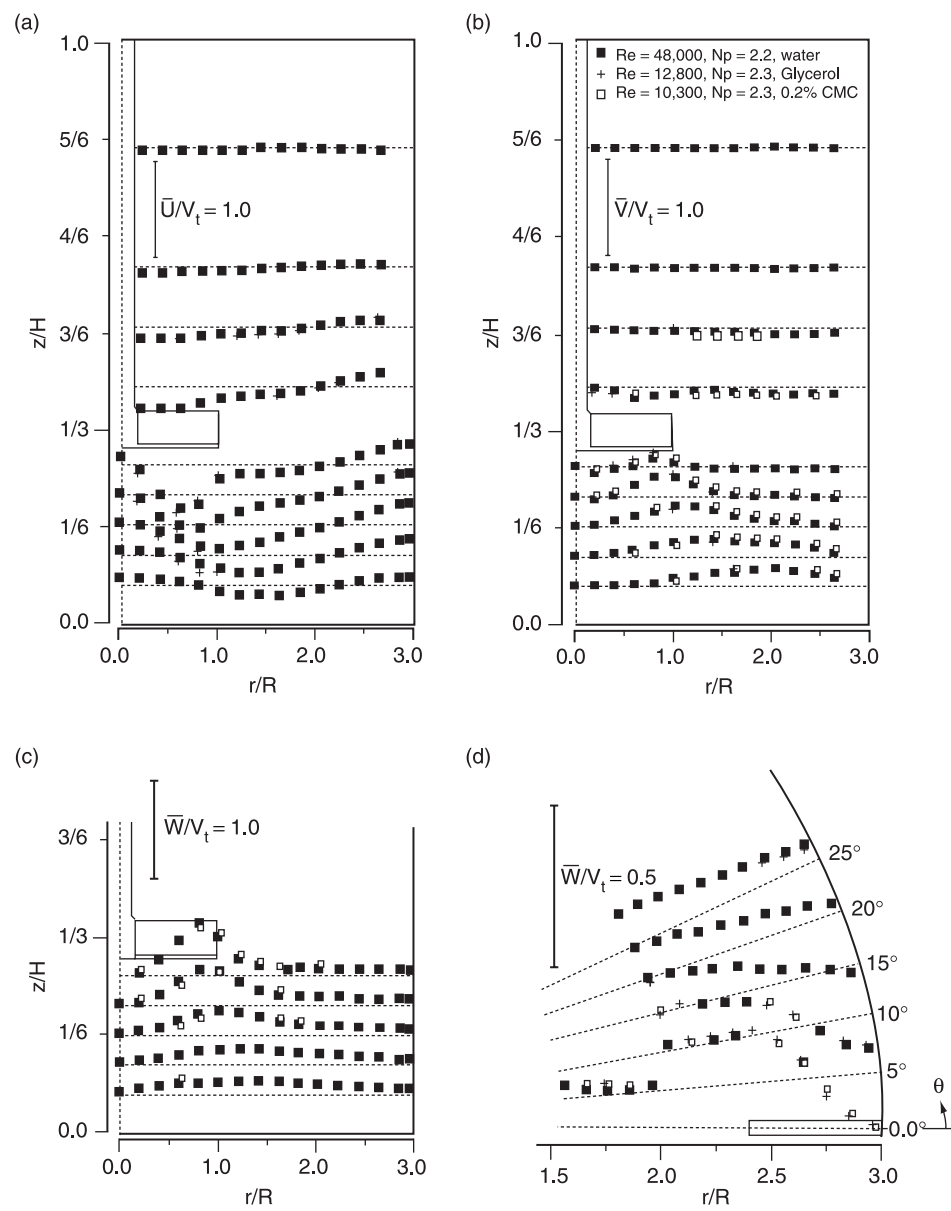


Figure 4 Comparison between the mean flow velocity profiles of Newtonian fluids and 0.2% CMC solution for a power number 2.3: (a) axial component in r-z plane & $\theta = 0^\circ$, (b) radial component in r-z plane & $\theta = 0^\circ$, (c) tangential component in r-z plane & $\theta = 0^\circ$, (d) tangential component in r- θ plane & $z = 0.068H$.

solution are larger by 5, 2 and 3% of the tip velocity, respectively. Elsewhere, the rms velocities with glycerin and CMC solutions are similar to within 1% of the bulk velocity. Behind the baffle, figure 5(d), the rms of the tangential velocity with CMC solution is almost uniformly lower than with the glycerin solution by $0.019V_t$.

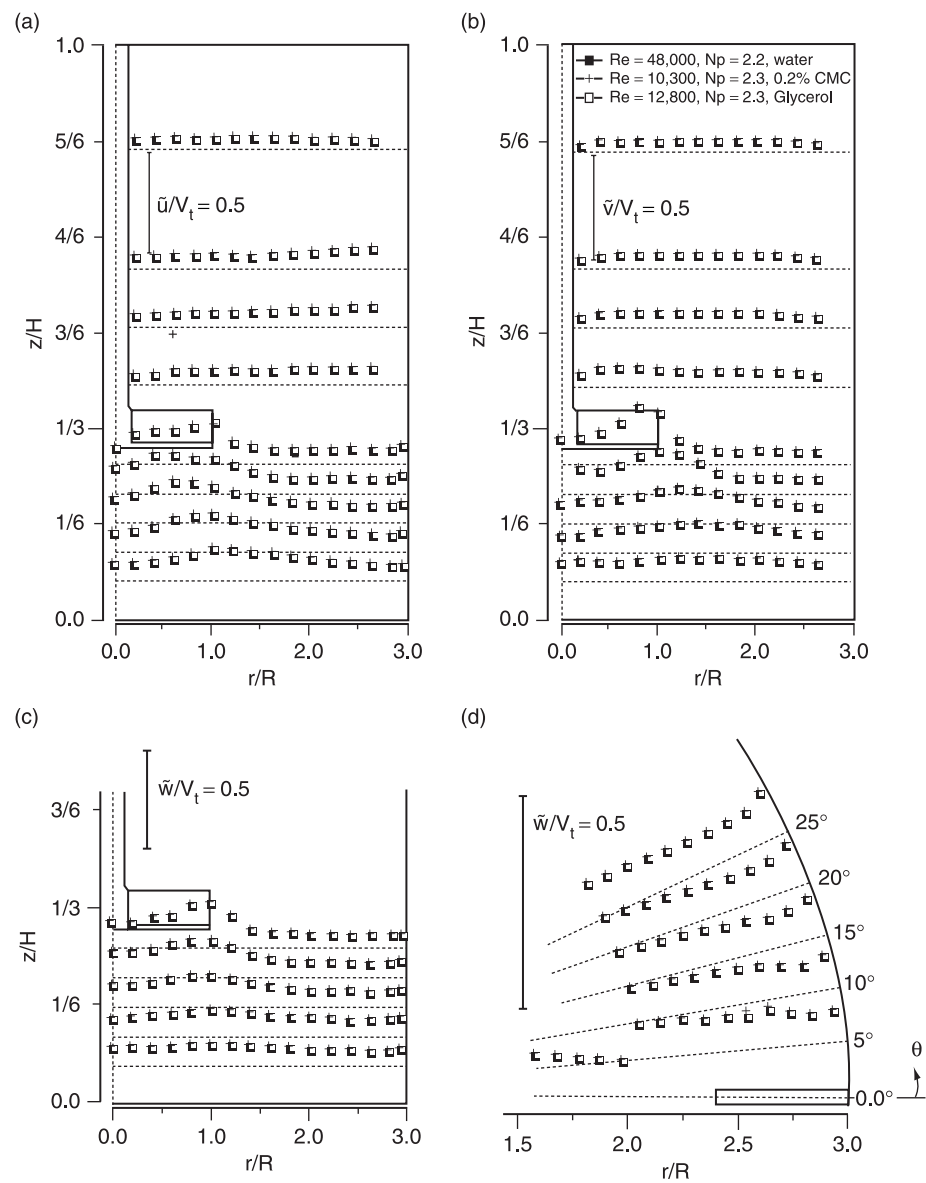


Figure 5 Comparison between the turbulence velocity fluctuation profiles of Newtonian fluid and 0.2% CMC solution: captions the same as in figure 4.

Figure 6 presents contours of the normalized turbulence kinetic energy, k/V_t^2 where $k = (\tilde{u}^2 + \tilde{v}^2 + \tilde{w}^2)/2$, with glycerin and CMC solutions below the impeller and confirms the overall suppression of turbulence with CMC flow. The maximum difference occurs in the impeller jet close to its tip and is of order of $0.018V_t^2$ that reduces to $0.002V_t^2$ near the wall.

Overall, the comparison of the turbulence quantities shows the two Newtonian flows operating at Reynolds numbers of 12,800 and 48,000 are more similar than the power number matched Newtonian and non-Newtonian CMC flows where some suppression of

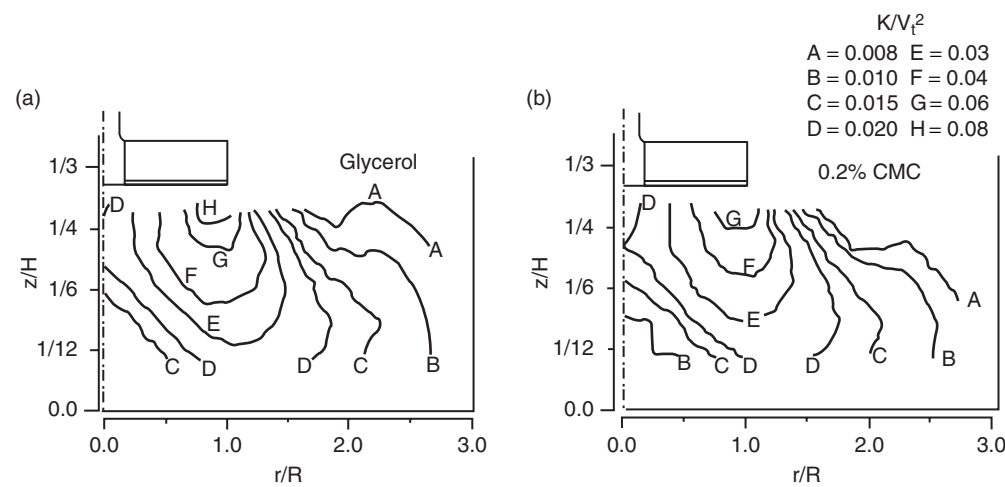


Figure 6 Distribution of the turbulence kinetic energy below the impeller for a power number 2.3 and $\theta = 0^\circ$: (a) Newtonian fluid, (b) 0.2% CMC solution.

turbulence with the CMC flow is evident. Nevertheless, the differences between the CMC and glycerin flows are relatively small, indicating that the 0.2% CMC flow is probably fully turbulent above a Reynolds number of 10,000 as defined by Newtonian flows. These small differences in the bulk of the flow are likely to have negligible effect on mixing times, although processes that depend on the micro-mixing for chemical reactions could be affected by differences in turbulent length scales and dissipation rates. The quantities could not be estimated here since the time between the individual measurements was not available and the data rate was too low, about 0.6 kHz; both quantities will be needed for future studies of the dissipation rate and characteristic length scales.

3.2.2. Measurements with respect to the impeller

All the velocity results presented hereafter are the ensemble-average values obtained over 1.08° intervals of impeller rotation. Measurements were made around the impeller at axial locations from $z' = 0.7B$ to $-0.97B$ and radial locations from $r = 0.31R$ to $1.12R$ where $z' = 0$ is the impeller centerline and B is the height of the blades which is 18.5 mm, please see figure 1. Since the flow characteristics of Newtonian fluid with respect to blade rotation were fully explained by [1], here the emphasis would be on the differences between the three flows (two Newtonian fluids and 0.2% CMC fluid). In order to show these more clearly, their mean velocity profiles with respect to impeller rotation, ϕ are plotted on the same graph and are presented in figures 7, 8 and 9 for axial locations of $z' = 0.7B$, $-0.7B$ and $-0.97B$, respectively.

Just above the impeller at $z' = 0.7B$, figure 7, and at a radius of $0.82R$ close to the impeller tip, the results of axial and radial mean velocities in the glycerin and CMC flows are quite similar to within $0.01V_t$ and the tangential velocity is similar up to a shaft angle of 30° , after which it is $0.05V_t$ greater in the CMC flow; at all other radial locations, the tangential velocity is greater by an average of $0.015V_t$. Comparison between the two Newtonian flows shows a decrease in axial velocity with Reynolds number of about $0.02V_t$, and a phase shift of 2° . The radial and tangential velocities of the two flows are similar to around $0.01V_t$; similar differences were found at other radial locations.

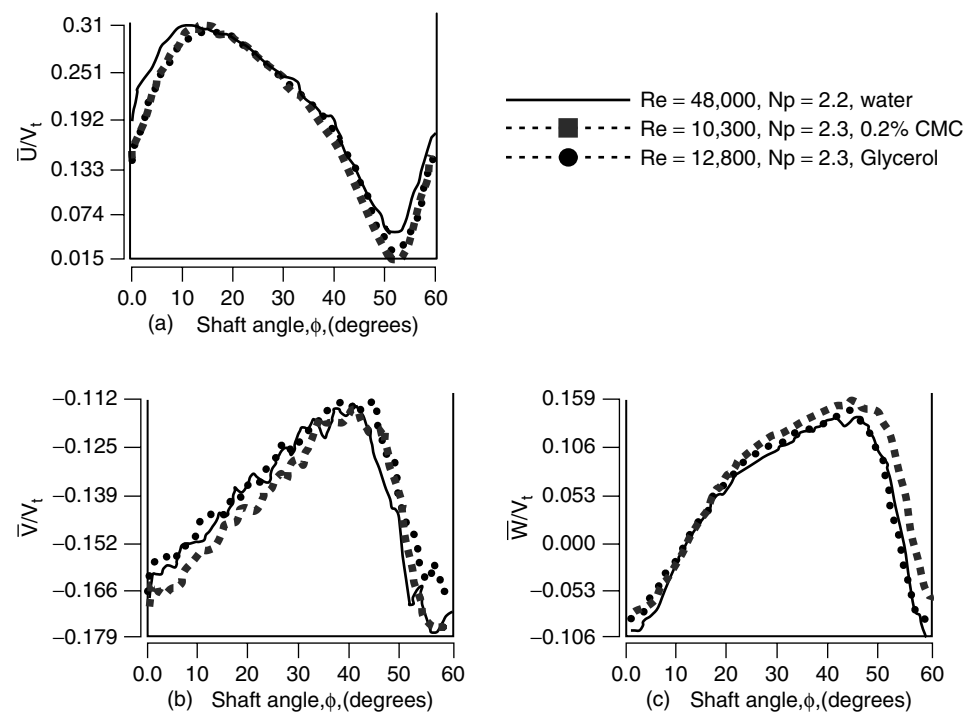


Figure 7 Comparison between the mean flow velocity profiles of Newtonian fluids and 0.2% CMC solution with respect to impeller rotation above the impeller at $z' = 0.7B$ and $r = 0.82R$: (a) axial component, (b) radial component, (c) tangential component.

The mean velocity variation of all three flows directly below the impeller in the discharge jet, $z' = -0.7B$, is shown in figure 8 at radial locations of $r = 0.61R, 0.82R, 0.92R$ and $1.02R$. A phase difference of 3 to 4 degrees between the Newtonian flows is present in all the velocity components and at all radial locations, where the flow at lower Reynolds number lags behind that at higher Reynolds number so that the abrupt swing of radial and tangential flow takes place further away from the blade trailing edge. The outward shift in the impeller jet with the lower Reynolds number is also evident from the axial velocities at various radial locations of figure 8(a). Other than the phase difference the axial, radial and tangential velocities are similar to within 3%, 5% and 2% of the tip velocities, respectively. With the two power number matched flows, all velocity components at almost all radial locations are similar to within one degree in terms of phase, and the impeller jet is shifted outwards in the CMC flow compared to the glycerin flow. This shift can be seen by comparing the axial flows at $r = 0.61R$ where the velocities are lower in the CMC flow, to that at $r = 0.92R$ or $r = 1.02R$, where the velocities are lower in the glycerin flow; this change of sign in axial velocities between the two flows are due to the viscosity variation of CMC solution as will be shown later when the viscosity is calculated.

As the flows convected further downward, $z' = -0.97B$, the differences in mean velocities between the three flows become even less as shown in figure 9 at a radius of $0.82R$. The phase difference of up to 4° in Newtonian flows with the lower Reynolds number lagging behind is evident. The peak axial and radial velocities in higher Reynolds number are greater than in the lower Reynolds number by about $0.02V_t$ and $0.04V_t$, respectively, while the

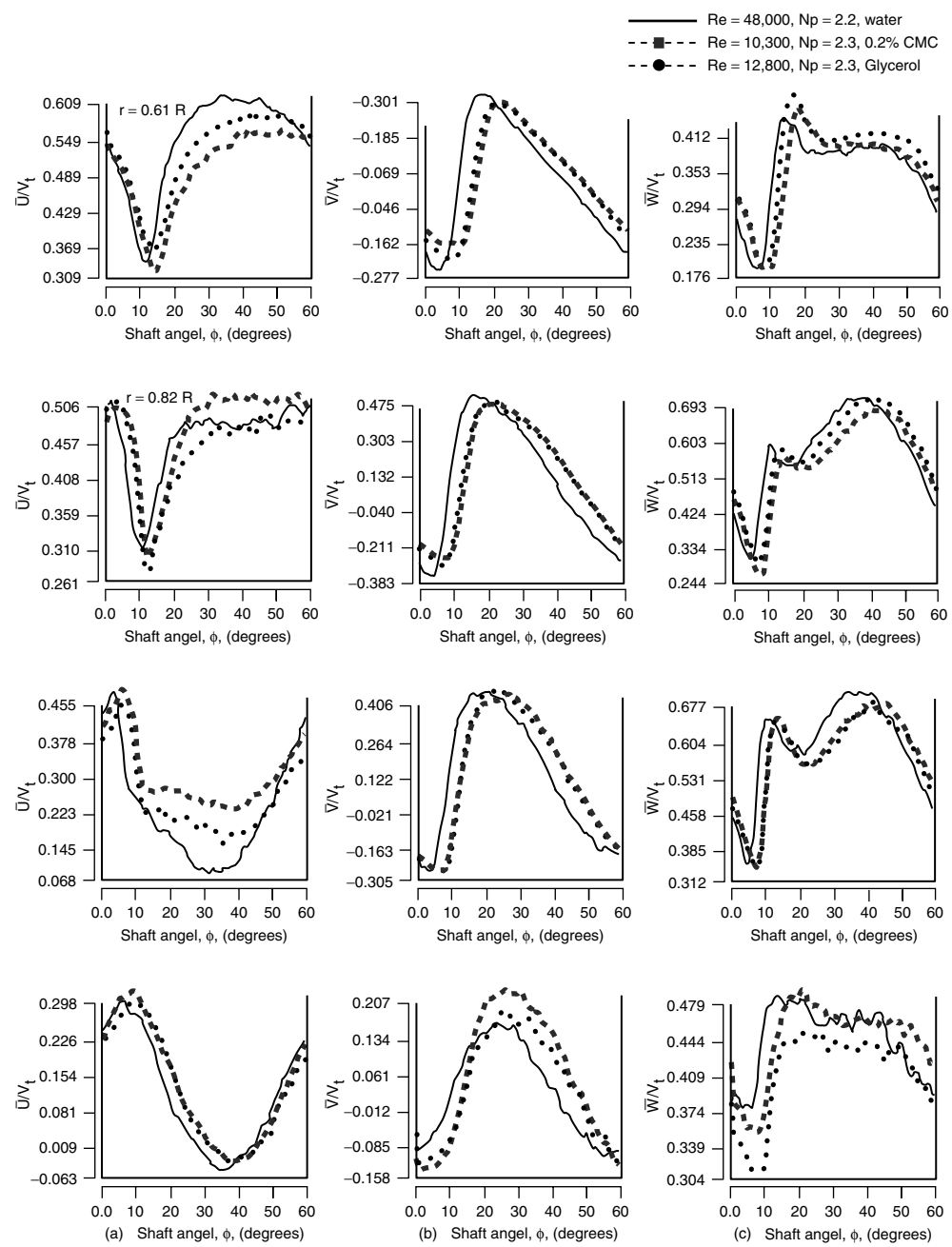


Figure 8 Comparison between the mean flow velocity profiles of Newtonian fluid and 0.2% CMC solution with respect to impeller rotation below the impeller at $z' = -0.7B$ and four radial positions of $r = 0.61, 0.82, 0.92$ and $1.02R$: (a) axial component, (b) radial component, (c) tangential component.

tangential components of two flows are similar. The CMC and glycerin flows have similar flow patterns and phase, with the CMC flow having $0.02V_t$ greater axial velocities; similar radial velocities and $0.02V_t$ lower tangential velocities than those in glycerin flow.

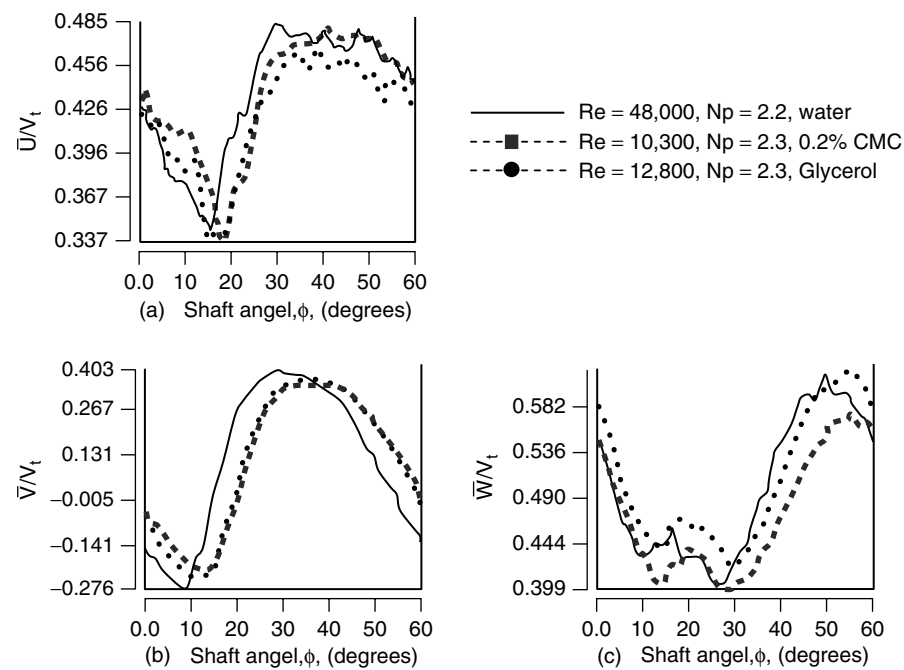


Figure 9 Comparison between the mean flow velocity profiles of Newtonian fluids and 0.2% CMC solution with respect to impeller rotation below the impeller at $z' = -0.97B$ and $r = 0.82R$: (a) axial component, (b) radial component, (c) tangential component.

Overall, the two power number matched flows are more similar in terms of mean velocities than the two Newtonian flows. The greatest difference between the Newtonian flows results from the four degrees phase lag and the outwards shift in the impeller jet at the lower Reynolds number. Again, the similarities in the Newtonian flows would be expected, as they are turbulent with Reynolds number above 10,000, so that the flow should be nearly invariant with Reynolds number.

Contours of the turbulence velocity fluctuation of all components directly below the impeller, $z' = -0.7B$, are presented in figures 10 for the glycerin and CMC flows. The results show similar distribution of velocity fluctuation with turbulence levels generally lower everywhere in the CMC flow. The rms values of the axial and tangential components are $0.065V_t$ lower and the radial component value $0.04V_t$ lower in the CMC flow near the edge of the blade. Elsewhere, the axial rms values are 0.01 to $0.05V_t$ lower and the radial and tangential values are $0.03V_t$ lower in the CMC flow. Comparison of the two Newtonian flows (see [1] for higher Reynolds number) shows similar distribution with a phase shift of about 3° similar to that of the mean flow and that the fluctuating turbulence levels are lower for the flow at the lower Reynolds number by up to $0.03V_t$.

The distribution of the turbulent kinetic energy, k , of the glycerin and CMC flows above and below the impeller are compared in figure 11 in contours form and, in general, shows similar distribution for both flows with an overall reduction in turbulence kinetic energy for the CMC flow. Just above the impeller, $z' = 0.7B$ of figure 11(a), the turbulence kinetic energy in the CMC flow is lower than glycerin flow by an average of $0.0015V_t^2$. Below the impeller in the discharge flow, however, the suppression of the turbulence is stronger in the CMC flow so that directly below the impeller, figure 11(b), the level of k is on average $0.02V_t^2$ lower

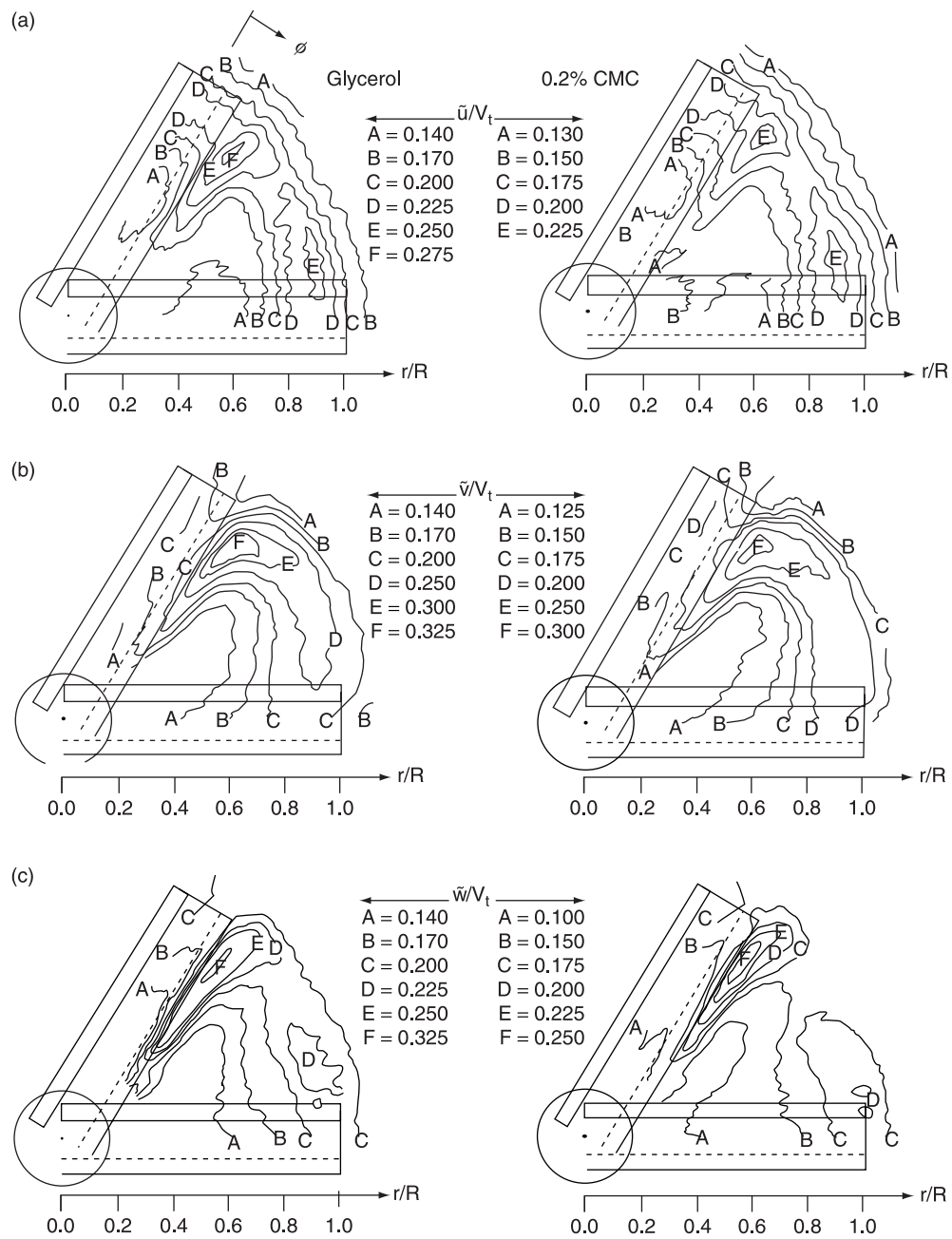


Figure 10 Distribution of the turbulence velocity fluctuations for Newtonian fluid and 0.2% CMC solution with respect to impeller rotation at $z' = -0.7B$ below the impeller: (a) axial rms velocity, (b) radial rms velocity, (b) tangential rms velocity.

in the CMC flow with the peak value some $0.045V_t^2$ lower near the edge of the blade. Further away from the blade at $z' = -0.97B$, figure 11(c), the CMC flow has turbulence kinetic energy levels generally about $0.025V_t^2$ lower than in glycerin flow, with a peak value $0.029V_t^2$ lower.

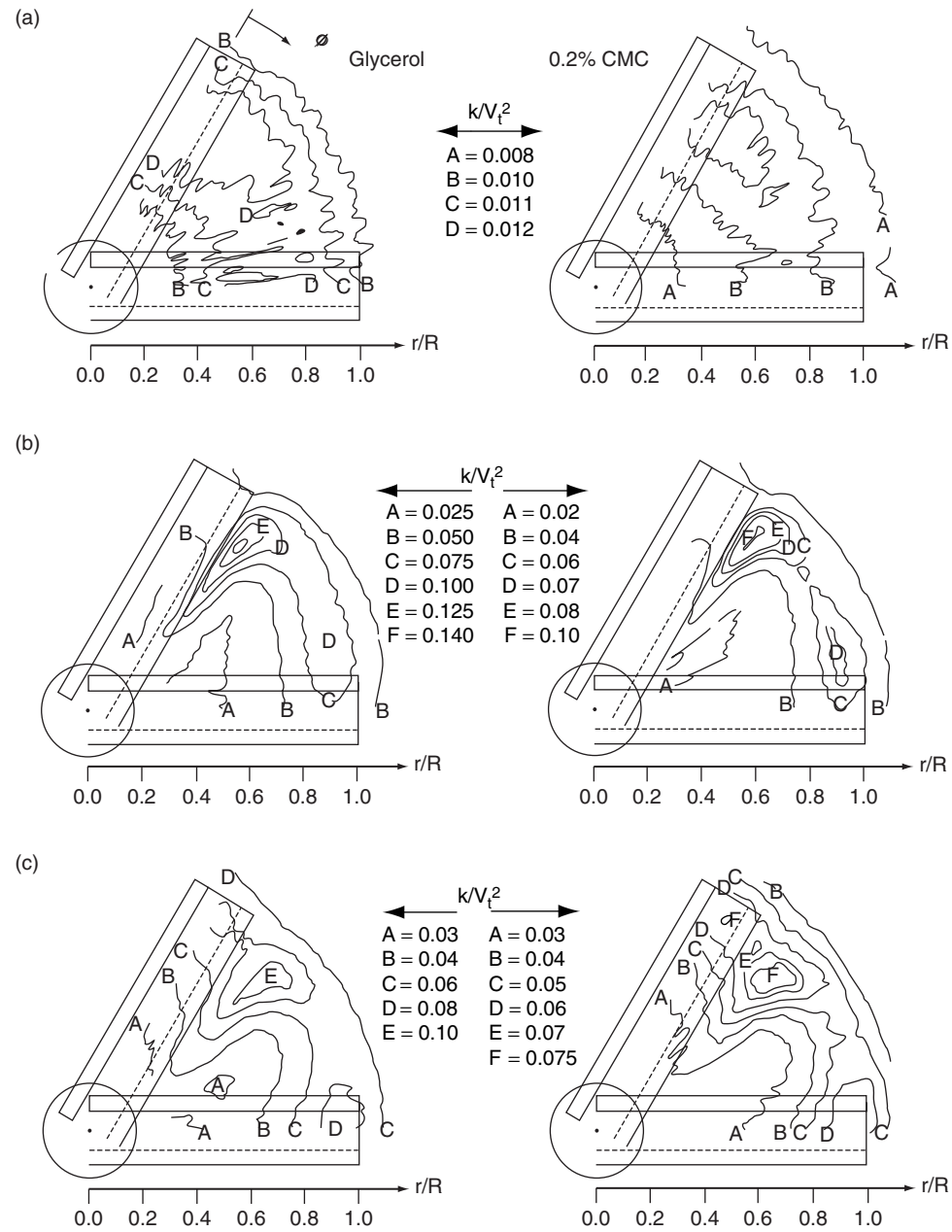


Figure 11 Distribution of the turbulence kinetic energy for Newtonian fluid and 0.2% CMC solution with respect to impeller rotation around the impeller: (a) $z' = 0.7B$, (b) $z' = -0.7B$, (c) $z' = -0.97B$.

Overall, large suppression of turbulence fluctuations is obtained by the CMC flow compared to that of the power number matched Newtonian flow so that in term of turbulence kinetic energy values are $0.0015V_t^2$ lower with the CMC flow in the inlet flow and 0.02 to $0.045V_t^2$ lower in the impeller jet. The differences in the turbulence quantities between the

two Newtonian flows are, however, much less than the two power number matched flows by at least a factor of two which showed slight increase in turbulence with Reynolds number; the turbulence kinetic energy was about $0.01V_t^2$ larger at the higher Reynolds number.

3.3. CALCULATED VALUES

The velocity data measured with respect to the impeller rotation were used to calculate the discharge coefficient, and to perform a mass and energy balance on the impeller. The strain rate generated by the three flows was also calculated from which the apparent viscosity of the CMC solution was estimated. The procedure for these calculations was fully described by [1] and will not be repeated here except for the calculation of the strain rate.

The performance of an impeller can be best characterised with power number, N_p , and the coefficient of discharge, $K_d = Q/\rho ND^3$ where Q is the discharge mass flow rate, which is a measure of pumping capacity of the impeller. The calculated discharge mass flow rate for all three flows are listed in table 1 which gave rise to values of $K_d = 0.88, 0.88$ and 0.89 for the water ($Re = 48,000$), glycerin ($Re = 12,800$) and CMC flows, respectively. These values provide a good indication of the similarity in the normalised mean velocities observed in previous sub-sections and suggest there is little difference in mixing times between the flows. The corresponding pumping efficiencies (or the hydraulic efficiency, defined as K_d/N_p , which is a measure of effectiveness of the impeller for generating mean flow per unit of power input) are found to be $0.4, 0.4$ and 0.39 , indicating there is little difference between the flows in term of flow rate per unit energy input. Therefore, for a flow-controlled mixing process, the impeller is acting with almost the same mixing efficiency for all flow conditions and fluids.

Table 1 Pitched blade impeller mass and energy balance

	Water flow	Glycerin flow	CMC flow
Torque balance			
Calculated power number, N_p	2.36	2.39	2.44
Measured power number, N_p	2.2	2.21	2.3
Mass balance			
Mass flow in (kg/s)	4.11	11.4	10.0
Mass flow out (kg/s)	4.14	12.6	11.2
Coefficient of discharge, K_d	0.88	0.88	0.89
Hydraulic efficiency, K_d/N_p	0.4	0.4	0.39
Energy balance			
% Dissipated within impeller region	2	6	15
% Converted into mean flow	70	68	66

The strain rate based on mean velocity gradients was also calculated as another means of comparing the macro-mixing capabilities of the three flows. The mean velocity was measured along the discharge plane of the impeller every 5mm in the radial direction, at axial locations $z' = -13\text{mm} (-0.7B)$ and $-18\text{mm} (-0.97B)$ to form control volumes of $5\text{mm} \times 5\text{mm} \times 1.08^\circ$, and velocity gradients were found at the mid-point of each control volume. The size of these control volumes may be too large to estimate the strain rate with an accuracy of better than, say 15%, but the method allows a comparison to be made between the three flow conditions. The strain rate, independent of the coordinate axes orientation, is equal to half the square-root of the second invariant of the strain tensor, $\sqrt{II\gamma/2}$, where the second invariant $II\gamma$ is

$$\begin{aligned}
 II_{\gamma} &= \sum_i \sum_j \dot{\gamma}_{ij} \dot{\gamma}_{ji} \\
 &= 4 \left[\left(\frac{\partial U}{\partial z} \right)^2 + \left(\frac{\partial V}{\partial r} \right)^2 + \left(\frac{1}{r} \frac{\partial W}{\partial \phi} + \frac{V}{r} \right)^2 \right] + 2 \left(\frac{\partial V}{\partial z} + \frac{\partial U}{\partial r} \right)^2 \\
 &\quad + 2 \left(r \frac{\partial}{\partial r} \left(\frac{W}{r} \right) + \frac{1}{r} \frac{\partial V}{\partial \phi} \right)^2 + 2 \left(\frac{1}{r} \frac{\partial U}{\partial \phi} + \frac{\partial W}{\partial z} \right)^2
 \end{aligned} \tag{3}$$

The strain rate was normalised by the impeller angular velocity, ω , and the results for the three flows are presented in figure 12 in contour form. All flows produce similar patterns of strain rate with the highest values along the trailing edge of the blade at $r = 0.62$, where the mean flow swings abruptly from a radially inwards to outwards flow, as was described by [1], and in the tip vortex at $r \approx 0.9R$ and $\theta = 50^\circ$; the minimum values are at the end of the

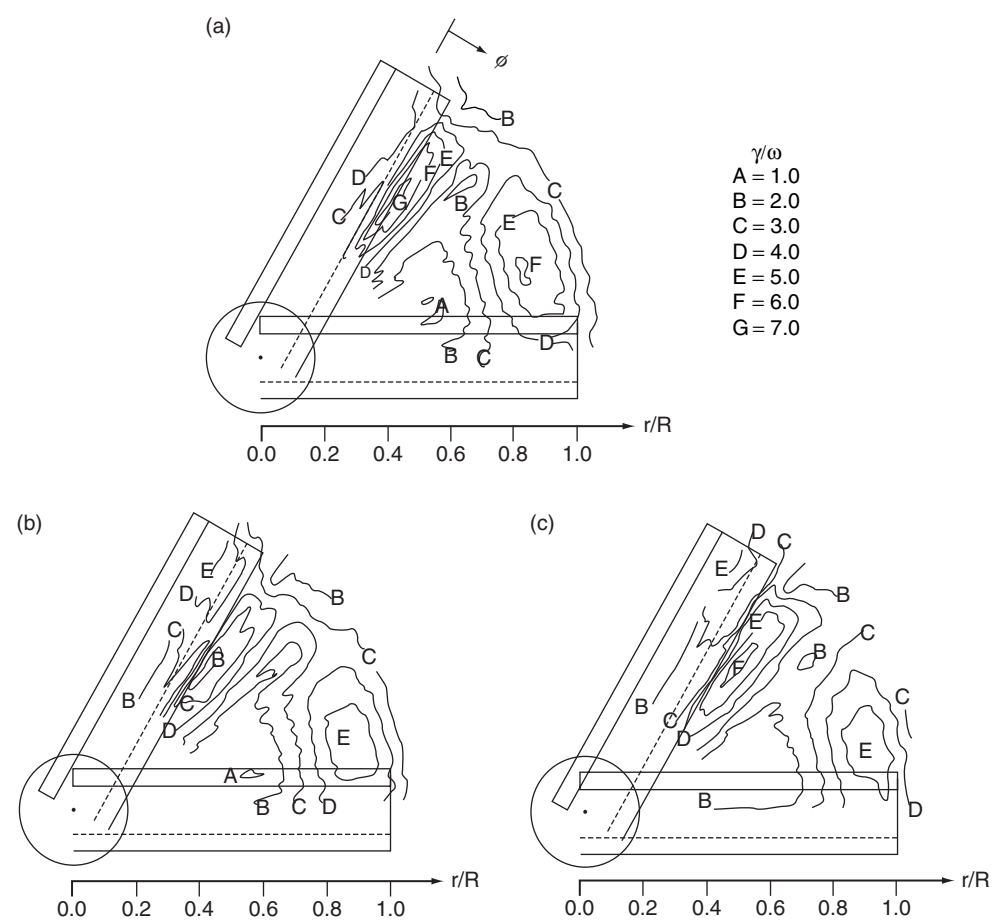


Figure 12 Distribution of the contours of the strain rate with respect to impeller rotation at $z' = -0.7B$: (a) Water flow, (b) Glycerol flow, (c) 0.2% CMC flow.

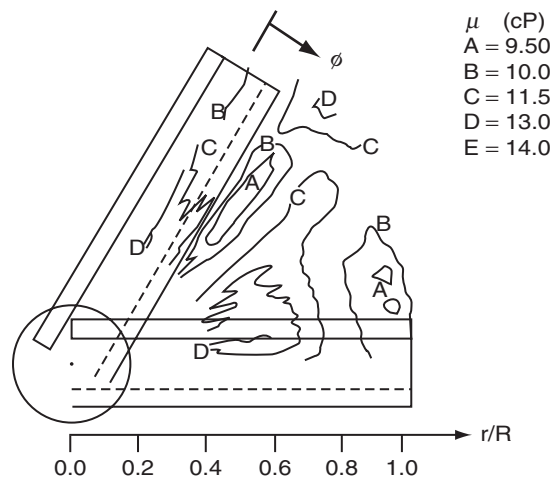


Figure 13 Variation of apparent viscosity for 0.2% CMC solution with respect to impeller rotation at $z' = -0.7B$.

blades close to the impeller shaft towards the blade's leading edge. The maximum strain rate for the water flow, figure 12(a), was 7ω along the blade and 6ω in the tip vortex, with values dropping to 1ω close to the shaft and 3ω beyond the impeller tip. The study of [23] showed that the tip vortex plays an important role in the liquid-liquid drop break-up process, which is probably due to the presence of the high strain rates there as was demonstrated above.

The maximum strain rate with glycerin flow, figure 12(b), is 1ω lower than in the water flow with similar values elsewhere, although the phase difference observed in the mean flows (about 3 to 4 degrees) is also evident here. The strain rates variation and magnitude in the CMC flow, figure 12(c), is quite similar to those in glycerin flow except a slight phase shift in the peak strain rate of the CMC flow away from the trailing edge. The strain rate variation in CMC flow over the impeller cycle will cause a change in the apparent viscosity that was calculated and presented in figure 13. A variation of up to 50% is evident, from a minimum viscosity of 9.5 cP in the region of the highest strain rate, close to impeller tip, to a maximum value of 14cP in the region of the lowest strain rate, close to the impeller shaft. The variation of apparent viscosity may have contributed to outward shift of the impeller jet noted in figure 8 since the viscosity of the CMC solution is lower than the viscosity of the glycerin solution (11.5 cP) towards the impeller tip causing higher axial velocity, while the viscosity is higher towards the impeller shaft with lower axial velocity. The results suggest that in the mixing systems where the mean flow strain rate is important, the mixing effectiveness will increase slightly with Reynolds number, and there would probably be little difference between the glycerin and CMC flows.

The shaft power input to the impeller was calculated from the velocity measurements by performing a torque (angular momentum) balance around the impeller in the same manner described by [1] and the results are given in table 1 together with the measured values from the air bearing. The agreement between the measured and calculated values with all flows was good, with a maximum difference of 7.5% in the case of glycerin flow, considering the errors involved in the integration of velocity profiles, in the blade to blade velocity differences since every 60° interval was assumed to be the same, in the LDV measurements, and finally errors incurred in the torque measurements. This is also a good indication of the



velocity measurements accuracy and provides confidence in the results. A further check of velocity measurements was provided by mass flow balance, table 1, with the in-flow (along the top and side of the impeller) matching the out-flow (along the bottom) to within 1% for the water flow and 11% for the glycerin and CMC flows.

Many mixing systems are dependent upon small-scale turbulence to enhance mixing and therefore rates of chemical reaction, heat and mass transfer [24]. The effectiveness of the impeller in generating small-scale turbulence can be estimated by a balance of mean and turbulent kinetic energy flowing through the impeller, neglecting the cross-correlation terms, and then an estimate of the energy dissipation within the impeller can be obtained by comparing the net gain in kinetic energy through the impeller to that of power input to the impeller, assuming the potential energy and pressure work are negligible; the results are listed in table 1. It should be noted that due to assumptions made and also measurement errors, the calculated values are not absolute but a good indication as what are happening with the right order of magnitudes. Comparison of the two Newtonian flows shows little variation with Reynolds number in the proportions of energy converted into the mean flow and turbulence, although there is an indication that less energy is dissipated within the impeller at the higher Reynolds number.

Although the glycerin and CMC flows, with the same power input, convert similar proportions into mean flow production, the CMC flow dissipates 9% more energy within the impeller region and as a consequence less energy goes into turbulence production. Therefore, for the mixing system where the micro-mixing is important the impeller operates less effectively in the CMC flow compared to a Newtonian flow at a similar power number. Polymer additives, and CMC in particular, are known to cause drag reduction in the turbulent pipe and annular flows compared to the flows of a Newtonian solvent [20, 25, 26, 27, 28] who showed a dampening of the turbulence, especially in the cross-stream components, and also a change in the turbulence spectrum [29]. It has been suggested by [21] that this is caused by an increase in elongational viscosity of the fluid when the polymer molecules stretch under the influence of normal strain. This phenomenon has probably caused the higher power dissipation and lower turbulence production in the CMC flow compared to that of the glycerin flow.

4. CONCLUSION

Three mean velocity components and the corresponding rms velocities generated by a 60° pitched blade impeller in a standard fully baffled mixing vessel have been measured by laser Doppler velocimetry. A Newtonian fluid (glycerin solution) at a Reynolds numbers of 12800, and a power number matched shear-thinning polymer solution (0.2% CMC) has been investigated. Comparison was also made with a Newtonian water flow at a Reynolds number of 48,000 [1]. The more important findings are as follow.

The bulk velocity measurements, resolved over many impeller rotation, showed that the mean and rms velocities of the two Newtonian flows were similar with maximum differences of $0.05V_t$ and $0.03V_t$, respectively, in the impeller jet. The mean velocity similarity of the two power number matched flows was even better than the two Newtonian flows with a maximum difference of $0.03V_t$ in the impeller jet. However, the turbulence intensity of the CMC flow was generally lower than the glycerin flow by $0.05V_t$ for the axial rms velocity and up to $0.03V_t$ for the radial and tangential rms velocities in the impeller jet, elsewhere in the vessel the rms values were lower by up to $0.02V_t$.

Similar trends in mean and rms velocities were obtained around the impeller from the velocity measurements with respect to the impeller rotation, resolved over 1.08° . The results



showed a phase difference between the two Newtonian flows of 3 to 4° with the impeller jet shifted slightly towards the tip in the glycerin flow. The glycerin and 0.2% CMC flows were again more similar in terms of mean velocities than the two Newtonian flows, and were in phase to within 1°, and that the impeller jet was shifted slightly towards the tip in the CMC flow. The turbulence kinetic energy level was lower for the CMC flow by about $0.02V_t^2$.

The calculated values of the discharge coefficient and the energy balance indicated that the pitched blade impeller generates mean flow with similar pumping efficiency, about 0.4 per unit power input, for all flow conditions so that there would be little difference in mixing times between the three flows. The calculated strain rate based on mean flow gradients showed a maximum value of 7ω in the water flow below the impeller along the blade edge which was 1ω higher than that of lower Reynolds number glycerin flow; the strain rates in glycerin and CMC flows were found to be similar. The results suggest that for mixing processes where the shear rate is important, the efficiency should improve slightly with Reynolds number, and there should be little difference between the power number matched glycerin and CMC flows.

The energy balance around the impeller showed that for Newtonian flows less than 6% of the input energy was dissipated within the impeller region, about 70% was converted into the mean flow and 25% went into the turbulence production. In the CMC flow, however, 9% more of the total input power was dissipated within the impeller and 7% less went into the turbulence compared to the power number matched Newtonian flow, indicating that the impeller operates less effectively in CMC for mixing processes where the micro-mixing is important. This higher energy dissipation in the CMC flow is probably due to the mechanism that is also responsible for drag reduction in duct flows.

NOTATION

B	Blade height, m
C	Impeller clearance from the bottom of the tank, m
D	Impeller diameter, m
H	Liquid height in the tank, m
k	Turbulence kinetic energy ($= [\tilde{u}^2 + \tilde{v}^2 + \tilde{w}^2]/2$)
k_s	The shearing constant
K_d	Coefficient of discharge ($= Q/\rho ND^3$)
m	Fluid consistency, $\text{pa}\cdot\text{s}^{-n}$
n	Power law index of the fluid
N	Impeller rotational speed, rev s^{-1}
N_p	Power number $\left(= \frac{P}{\rho N^3 D^5} \right)$
P	Power consumed, N m s^{-1} ($= \omega T_r$)
Q	The discharge mass flow rate, kg s^{-1}
r	Radial distance from the centre of the tank
R	Impeller radius, m
Re	Reynolds number $\left(= \frac{ND^2}{\nu} \right)$
T	Tank diameter, m
T_r	Induced torque, N m
\tilde{u}	Axial rms velocity, m s^{-1}



\bar{U}	Axial mean velocity, m s ⁻¹
\tilde{v}	Radial rms velocity, m s ⁻¹
\bar{V}	Radial mean velocity, m s ⁻¹
\bar{V}_t	Impeller tip velocity, m s ⁻¹ ($= \pi ND$)
\tilde{w}	Tangential rms velocity, m s ⁻¹
\bar{W}	Tangential mean velocity, m s ⁻¹
z	Axial distance from the bottom of the tank
z'	Axial distance from the impeller centre-line

GREEK LETTERS

α	Pitch to diameter ratio
ϕ	Angular position of the blade, degree
$\dot{\gamma}$	Strain rate, s ⁻¹ ($= k_s N$)
μ	Dynamic viscosity, Pa.s
ν	Fluid kinematic viscosity, m ² s ⁻¹
θ	Angular plane with respect to baffle position, degree
ρ	Fluid density, kg m ⁻³
ω	Impeller angular velocity, rad s ⁻¹

REFERENCES

- [1] Hockey, R. M. and Nouri J.M., *Turbulent flow in a baffled vessel stirred by a 60° pitched blade impeller*, *Chemical Engineering Science*, **51**, 4405–4421, 1996.
- [2] Armstrong, S.G. and Ruszkowski, S., *Measurement and comparison of flows generated by different types of impeller in a stirred tank*, *Proc. of Colloquium on Mechanical Agitation, Toulouse, France*, 1987, 1.9–1.16.
- [3] Ranade, V.V. and Joshi, J.B., *Flow generated by pitched blade turbines I: measurements using laser Doppler anemometer*, *Chem. Eng. Comm.* **81**, 197–224, 1989.
- [4] Jaworski, Z., Nienow, A.W., Koutsakos, E., Dyster, K., and Bujalski, W., *An LDA study of turbulent flow in a baffled vessel agitated by a pitched blade turbine*, *Trans. IChemE.* **69**, 313–320, 1991.
- [5] Kresta, S.M., and Wood, P.E., *The mean flow field produced by a 45° pitched blade turbine: changes in the circulation pattern due to off bottom clearance*, *The Canadian J Chem. Eng.*, **71**, 42–53, 1993.
- [6] Sheng, J., Meng, H. and Fox, R.O., *A large eddy PIV method for turbulence dissipation rate estimation*, *Chemical Engineering Science*, **55**, 4423–4434, 2000.
- [7] Baldi, S. and Yianneskis, M., *On the quantification of energy dissipation in the impeller stream of a stirred vessel from fluctuating velocity gradient measurements*, *Chemical Engineering Science*, **59**, 2659–2671, 2004.
- [8] Solomon, J., Nienow, A. W. and Pace, G.W., *Flow patterns in agitated plastic and pseudoplastic viscoelastic fluids*, *IChemE Symp Series*, No. 64, A1–A13, 1981.
- [9] Solomon, J., Elson, T.P., Nienow, A.W. and Pace, G.W., *Cavern sizes in an agitated fluids with a yield stress*, *Chem. Eng. Com.*, **11**, 143–164, 1981.
- [10] Nouri, J.M. and Hockey R.M., *Power Number correlation between Newtonian and non-Newtonian fluids in a mixing vessel*, *J. Chem. Eng. of Japan*, **31**, 848–852, 1998.
- [11] Metzner, A.B. and Taylor, J.S., *Flow patterns in agitated vessels*, *A.I.Ch.E. Journal*, **6**, 109–114, 1960.

- [12] Greene, H.L. Carpenter, C. and Casto, L., 1982, *Mixing characteristics of an axial impeller with Newtonian and non-Newtonian fluids*, 4th European Conference on mixing, April 27–29 1982, Noordwijkerhout, Netherlands.
- [13] Metzner, A.B. and Otto, R.E., *Agitation of non-Newtonian fluids*, *A.I.Ch.E. Journal*, 3, 3–10, 1957.
- [14] Hockey, R.M., Nouri, J.M., and Pinho, F., *Flow visualisation of Newtonian and non-Newtonian fluids in a stirred reactor*. 3rd Int. Symp. of Flow Visualization, 1989, Prague.
- [15] Nouri, J.M. and Whitelaw, J.H., *Flow Characteristics of Stirred Reactors with Newtonian and Non-Newtonian Fluids*. *AIChE J.*, 36, 627–629, 1990.
- [16] Distelhoff, M.F.W., Laker, J., Marquis, A.J. and Nouri, J.M., *The application of a strain gauge technique to the measurements of power characteristics of five impellers*. *Experiment in Fluids*, 20, 56–58, 1995.
- [17] Carreau, P.J., Chhabra, R.P. and Cheng, J., *Effects of rheological properties on power consumption with helical ribbon impellers*, *A.I.Ch.E. Journal*, 39, 1421–1430, 1993.
- [18] Zhou, G., Tanguy, P.A. and Dubois, C., *Power consumption in a double planetary mixer with non-Newtonian and viscoelastic materials*. *Trans. IChemE.*, 78, 445–453, 2000.
- [19] Cavadas, A.S. and Pinho F.T., *Some characteristics of stirred vessel flows of dilute polymer solutions powered by a hyperboloid impeller*, *The Canadian J Chem. Eng.*, 82, 289–302, 2004.
- [20] Pinho, F.T. and Whitelaw, J.H., *Flow of non-Newtonian fluids in a pipe*. *J. Non-Newtonian Fluid Mechanics*, 34, 129–144, 1990.
- [21] Lumley, J.L., *Drag reduction in two phase and polymer flows*, *The Physics of Fluids*, 20, S64–S71, 1977.
- [22] Durst, F., Haas, R. and Interthal, W., *Laminar and turbulent flows of dilute polymer solution: a physical model*. *Rheo. Acta*, 21, 572–577, 1982.
- [23] Tatterson, G.B. and Stanford, T.G., *Liquid dispersion mechanisms in agitated tanks*, *Chem. Eng. Comm.*, 6, 371–376, 1981.
- [24] Uhl, V.W. and Gray, J.B., *Mixing: theory and application*, Academic Press, 1966.
- [25] Hoyt, J.W., *The effect of additives on fluid friction*, *ASME, J. Basic Eng.*, 94, 258–285, 1972.
- [26] Nouri, J.M., Umur, H. and Whitelaw, J.H., *Flow of Newtonian and non-Newtonian fluids in concentric and eccentric annuli*, *J. Fluid Mech.*, 253, 617–641, 1993.
- [27] Nouri, J.M. and Whitelaw, J.H., *Flow of Newtonian and non-Newtonian fluids in a concentric annulus with rotation of the inner cylinder*, *Trans. ASME. J. Fluid Eng.*, 116, 821–827, 1994.
- [28] Nouri, J.M. and Whitelaw, J.H., *Flow of Newtonian and non-Newtonian fluids in an eccentric annulus with rotation of the inner cylinder*, *Int. J. H. Fluid Flow*, 18, 236–246, 1997.
- [29] Allan, J.J., Greated, C.A. and McComb, W.D., *Laser-Doppler anemometer measurements of turbulent structure in non-Newtonian fluids*, *J. Phys. D: Appl. Phys.*, No. 17, 533–549, 1984.

ACKNOWLEDGEMENTS

The authors would like to thank the late Prof. J. H. Whitelaw of Imperial College and Dr F. Pinho of University of Porto for valuable discussions and helpful suggestions during the course of this work. Financial support from the EU, Unilever Research plc and ICI plc is gratefully acknowledged.

Copyright of International Journal of Multiphysics is the property of Multi-Science Publishing Co Ltd and its content may not be copied or emailed to multiple sites or posted to a listserv without the copyright holder's express written permission. However, users may print, download, or email articles for individual use.